COMMUNICATION

Chinese Journal of Structural Chemistry

An *In-Situ* Variable-Temperature Surface-Enhanced Raman Spectroscopic Study of the Plasmon-Mediated Selective Oxidation of *p*-Aminothiophenol

Wumei Cao[1], Yang Lu[1] and Yi-Fan Huang[1]*

[1]*School of Physical Science and Technology, ShanghaiTech University, Shanghai 201210, China*

ABSTRACT The roles of temperature change in surface-enhanced Raman scattering (SERS) hotspots are important for understanding the plasmon-mediated selective oxidation of *p*-aminothiophenol in a SERS measurement. Here, we demonstrate that the temperature change in hotspots seriously influences the conversion of *p*-aminothiophenol on Au by employing variable-temperature SERS measurements. The conversion steadily and irreversibly increased when the temperature increased from 100 to 360 K. But the conversion decreased above 360 K, because this conversion was exothermic. This temperature-dependence conversion suggests that the temperature change in hotspots originated from the photothermal effect should be coupled to the hot-electron effect in promoting the selective oxidation of *p*-aminothiophenol.

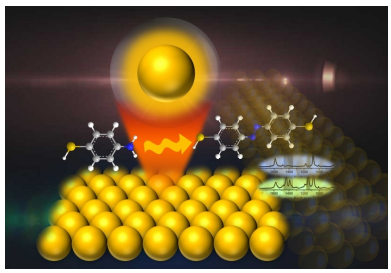

Keywords: surface-enhanced Raman spectroscopy, *p*-aminothiophenol, temperature, plasmon-mediated chemical reaction

n TEXT

Plasmon-mediated chemical reactions are promising in utilizing solar energy, because they use visible light for driving chemical reactions under mild conditions.[1-4] The oxidation of *p*-aminothiophenol (PATP) to *p,p'*-dimercaptoazobenzene (DMAB) during a surface-enhanced Raman spectroscopic (SERS) measurement is a typical plasmon-mediated chemical reaction, as shown in Equation 1, which occurs in an ambient condition under room temperature.[5-7] Similar reactions have been found regarding the conversions of aromatic anilines to azobenzene derivates.[8-10] Because the conversion of PATP is highly selective, it has been a model for investigating a plasmon-mediated chemical reaction in terms of plasmonic properties and reaction mechanisms.[11-14] So far, it is believed that hot electrons or holes are produced during plasmons decay and react with molecules on the surface of plasmonic materials.[3] The investigations by using a tip-enhanced Raman spectroscopy and a gap-mode SERS show that the localized surface plasmon boosts the conversion of PATP,[15-19] which are consistent with the conclusions from the laser-wavelength-dependent and laser-power-density-dependent observations.[12,20] The investigations about the mechanism of PATP conversion show that the molecular oxygen is activated by hot electrons and converted to surface oxygenated species, which selectively oxidizes PATP to DMAB.[21,22] Nonetheless, the temperature change in SERS hotspots caused by a photothermal effect is an important aftereffect of plasmons decay in addition to the production of hot electrons or holes,[3,23-26] which has been found in a SERS study of a plasmon-mediated chemical reaction of *p*-nitrothiophenol.[27-29] The missing understanding about the roles of temperature change in SERS hotspots makes the physical picture of the plasmon-mediated selective oxidation of PATP ambiguous, which is therefore desired to be revealed.

$$2\,\mathrm{AuS\text{-}Ph\text{-}NH_2} + \mathrm{O_2} + h\nu = \mathrm{AuS\text{-}Ph\text{-}N{=}N\text{-}Ph\text{-}SAu} + 2\mathrm{H_2O} \quad (1)$$

Here, we reveal the roles of the temperature change in SERS hotspots in the selective oxidation of PATP by using an *in-situ* variable-temperature SERS (VT-SERS). The measurements were carried out in a cell with a feedback-temperature-controlling system.[30] By reducing the laser power density in VT-SERS measurements, the photothermal effect, which is difficult to be directly measured, was excluded as much as possible. Thus, the temperature in SERS hotspots was manipulated through controlling the cell temperature, and the roles of temperature change in hotspots were revealed according to the temperature-dependent SERS spectra of PATP.

Figure 1 displays temperature-dependent surface-enhanced Raman spectra of PATP adsorbed on Au nanoparticles. The temperature gradually increased from 100 to 480 K. At 100 K, the main bands are at 1007, 1080, 1178, 1488 and 1590 cm^{-1}, which have been assigned to the characters of PATP.[31] At 280 K, the characteristic bands at 1142, 1388 and 1435 cm^{-1} appeared. Experiments and theoretical calculations in literatures assign these bands to the DMAB produced by PATP,[6-7,32] and thus the temperature of 280 K is the onset. Because the transformation process from PATP to DMAB depends on laser illumination time,[7,33] the spectral features are illumination-time-dependent. Therefore, to demonstrate the conversion of PATP under an equilibrium, the Raman spectra were acquired in a time serial at a fixed temperature. The spectra shown in Figure 1 are with laser-illumination-time-independent spectral features. Above 400 K, two broad bands appeared at the frequency span between 1300 and 1600 cm^{-1}, which are the spectral characters of amorphous carbon species.[32,34] The intensity of these two bands increased and those of other Raman bands decreased as the temperature increased up to 480 K, which shows a thermal decomposition of surface species.

In more details, the frequency of SERS bands was temperature dependent. For example, as shown in Figure 2a, the band of PATP steadily redshifted from 1080.4 to 1078.0 cm^{-1}, when the

DOI: 10.14102/j.cnki.0254-5861.2022-0134

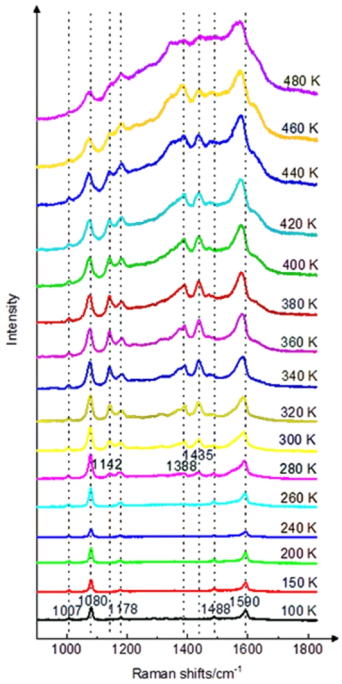

Figure 1. Temperature-dependent (from 100 to 480 K) Raman spectra of PATP adsorbed on Au nanoparticles excited by a 632.8 nm laser with a power density of 3.7 × 10^5 mW/cm^2.

temperature increased from 100 to 280 K. The redshift of SERS band can be ascribed to the temperature increase in SERS hotspots.[30] The intensity ratio of the bands of 1140 and 1080 cm^{-1} (I_{1140}/I_{1080}) was used to quantify the extent of the conversion of PATP. Figure 2b plots I_{1140}/I_{1080} as a function of temperature. In the SERS spectra of PATP and DMAB, the values of I_{1140}/I_{1080} are 0 and 2.34, respectively.[22] All values in Figure 2b fall between 0 and 2.34, indicating that not all PATP molecules were converted to DMAB. I_{1140}/I_{1080} steadily increased as a result of the increasing temperature from 280 to 360 K, which shows that the increase in the temperature in hotspots promoted the conversion of PATP.

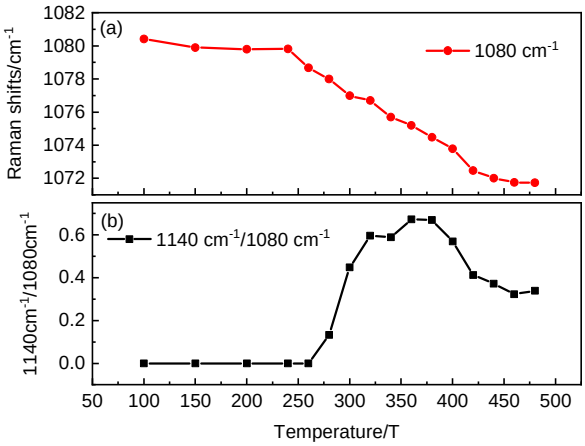

Figure 2. Temperature-dependent band frequency (a) and I_{1140}/I_{1080} (b) of PATP adsorbed on Au nanoparticles excited by a 632.8 nm laser with a power density of 3.7 × 10^5 mW/cm^2.

These temperature-dependent SERS of PATP indicate that the temperature in hotspots was well manipulated and the temperature change seriously influences the conversion of PATP.

It is interesting that I_{1140}/I_{1080} decreased when the temperature was higher than 360 K. The decrease in I_{1140}/I_{1080} indicates a backward conversion of DMAB, which is supported by a temperature-dependent SERS spectra in a cooling process. As shown in Figure 3, the temperature firstly increased from 100 to 360 K and then decreased backward to 100 K. It can be found that spectral features remain during the temperature dropping, which indicates that the increase in the intensity of the bands at 1140, 1390 and 1438 cm^{-1} between 280 and 360 K was not from any reversible temperature-dependent physical process, and was not changed in any further laser-illumination. Thus, the backward conversion of DMAB above 360 K is due to the decomposition of DMAB.

These temperature-dependent SERS spectra demonstrate that the conversion of PATP is a combination of a kinetics effect and a thermodynamics effect, which is supported by the density functional theory (DFT) calculations about the potential energy of elementary steps. Previous experiments suggest that the molecular oxygen activation to produce surface oxygenated species is the initial step which is followed by an oxidation of PATP.[22] Therefore, we examined two elementary steps, *i.e.* the reaction between a clean Au(111) slab surface and an oxygen molecule, and that between PATP and surface oxygenated species. The configuration of DMAB adsorbed on the Au(111) slab was similar to that on a Ag(111) one.[35] To demonstrate a representative tendency, the surface oxygenated species with a series of coverages was taken into account. Figure 4 summarizes the potential energy of the species in these two steps. The energy difference of the species before and after the conversion of PATP show that the net reaction energy was approximately -1.57 eV. On all Au(111)-O_n surfaces with an oxygen coverage from 2/3 to 2/9, the reaction energy values of the first step were positive and that of the second step was

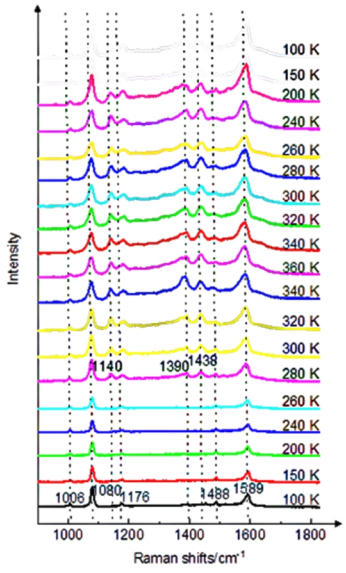

Figure 3. Temperature-dependent (between 100 and 360 K) Raman spectra of PATP adsorbed on Au nanoparticles excited by a 632.8 nm laser with a power density of 3.7 × 10^5 mW/cm^2.

DOI: 10.14102/j.cnki.0254-5861.2022-0134

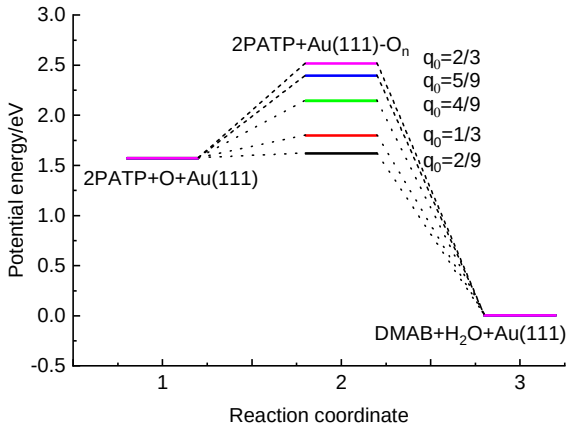

Figure 4. Oxygen-coverage-dependent potential energy of the conversion of PATP to DMAB calculated by using a DFT method.

negative. The production of oxygenated species was endothermic and the oxidation of PATP was exothermic. Based on these estimations about reaction energy, the influence of temperature change in the conversion of PATP as summarized in Figure 1 can be interpreted. When the temperature increased from 100 to 360 K, the conversion of PATP was trigged and promoted kinetically. Because the overall reaction of PATP is exothermic, further increase in temperature above 360 K led to a backward shift of the equilibrium of this reaction.

These understandings of the influence of a temperature change in the conversion of PATP demonstrate a clearer physical picture about the conversion of PATP in a SERS measurement. The laser of a Raman spectrometer excites the localized surface plasmons of a SERS substrate. Due to the localized surface plasmons, an enhanced electromagnetic field and the enhanced Raman scattering of surface species are generated. The decay of localized surface plasmons produces hot electrons and heat. The generated hot electrons effectively reduce the reaction barrier of activating molecular oxygen, which produces surface oxygenated species. The heat promotes the reaction between PATP and surface oxygenated species. The generations of hot-electrons and heat depend on the properties of a plasmonic material, and the reaction barrier between PATP and surface oxygenated species relies on the catalytic activity of a plasmonic material surface.

n CONCLUSION

In conclusion, the roles of temperature change of SERS hotspots in the plasmon-mediated selective oxidation of *p*-aminothiophenol to *p,p'*-dimercaptoazobenzene on Au were revealed at the temperature above 100 K by using a variable-temperature surface-enhanced Raman spectroscopy. In the laser illumination with a power-density of 3.7×10^5 mW/cm^2, the conversion of PATP steadily increased with an onset temperature of 280 K as it increased from 100 to 360 K. Further increase in temperature led to a backward shift of the conversion equilibrium of PATP. Density functional theory calculations show that the activation of molecular oxygen to surface oxygenated species is endothermic, and the reaction between PATP and the surface oxygenated species as well as the overall conversion between PATP and molecular oxygen is exothermic. These results suggest that the driving force of the conversion of PATP in a SERS measurement should be a synergistic effect of a photoelectric effect and a photothermal effect thermodynamically and kinetically, which is highly dependent on the plasmonic properties and the surface catalytic activity of a plasmonic material.

n EXPERIMENTAL

Au nanoparticles were synthesized according to Frens' recipe.[36] (See Supplementary information) The setup of variable-temperature SERS measurements was composed by Linkam THMS600 and a Renishaw In-Via Raman spectrometer, where a He-Ne laser with a wavelength of 632.8 nm was used.

The computation was performed by using a slab model based DFT calculation in the Vienna Ab-initio Simulation Package (VASP, version 5.4.1),[37,38] where the projector augmented wave method and Perdew-Burke-Ernzerhof generalized-gradient approximation functional were used.[39] An energy cutoff of 450 eV and a first order Methfessel-Paxton[40] smearing with a sigma of 0.2 were applied. The reaction energy change was approximately estimated by accounting the change in the energy of the electron. A five-layer Au(111) slab was applied, where three layers were fixed for simulating the properties of the bulk, and two layers of Au and adsorbate were fully optimized. A vacuum layer with a thickness of 30 Å was used for simulating the surface. PATP and DMAB were adsorbed on a Au(111)-6 × 3 slab, respectively. The O was adsorbed on a Au(111)-3 × 3 slab. A Monkhorst-Pack k-point sampling[41] of 5 × 5 × 1 was used. The dipole moment perpendicular to the surface was corrected. The lattice constant of Au is 4.174 Å.[42] The species of H_2O and O_2 was calculated by using a 10 Å × 10 Å × 10 Å cell with a 1 × 1 × 1 k-point sampling where the molecules are as in the gas phase. The spin-polarization was applied in the calculation of O_2. The reaction energy change was calculated by using the energy of the species with the optimized structure.

n ACKNOWLEDGEMENTS

This work was financially supported by the National Natural Science Foundation of China (Nos. 21872094, 21991152, and 21991150) and a ShanghaiTech University Start-Up grant. The HPC Platform of ShanghaiTech University Library and Information Services is acknowledged for the use of its supercomputer facilities.

n AUTHOR INFORMATION

Corresponding author. Email: huangyf@shanghaitech.edu.cn (Yi-Fan Huang)

n AUTHOR CONTRIBUTION

W.C. and Y.L. synthesized and characterized the nanoparticles, and performed the VT-SERS measurement; Y.F.H. performed the quantum chemistry calculations; all authors interpreted the data and cowrote the manuscript; Y.F.H. conceived the idea for this study.

n COMPETING INTERESTS

DOI: 10.14102/j.cnki.0254-5861.2022-0134

The authors declare no competing interests.

n ADDITIONAL INFORMATION

Supplementary information is available for this paper at http://manu30.magtech.com.cn/jghx/EN/10.14102/j.cnki.0254-5861.2022-0134

For submission: https://www.editorialmanager.com/cjschem

n REFERENCES

(1) Brus, L. Noble metal nanocrystals: plasmon electron transfer photochemistry and single-molecule raman spectroscopy. *Acc. Chem. Res.* **2008**, 41, 1742-1749.

(2) Linic, S.; Christopher, P.; Xin, H.; Marimuthu, A. Catalytic and photocatalytic transformations on metal nanoparticles with targeted geometric and plasmonic properties. *Acc. Chem. Res.* **2013**, 46, 1890-1899.

(3) Brongersma, M. L.; Halas, N. J.; Nordlander, P. Plasmon-induced hot carrier science and technology. *Nat. Nano* **2015**, 10, 25-34.

(4) Moskovits, M. The case for plasmon-derived hot carrier devices. *Nat. Nano* **2015**, 10, 6-8.

(5) Wu, D. Y.; Liu, X. M.; Huang, Y. F.; Ren, B.; Xu, X.; Tian, Z. Q. Surface catalytic coupling reaction of p-mercaptoaniline linking to silver nanostructures responsible for abnormal sers enhancement: a DFT study. *J. Phys. Chem. C* **2009**, 113, 18212-18222.

(6) Fang, Y.; Li, Y.; Xu, H.; Sun, M. Ascertaining p,p′-dimercaptoazobenzene produced from p-aminothiophenol by selective catalytic coupling reaction on silver nanoparticles. *Langmuir* **2010**, 26, 7737-7746.

(7) Huang, Y. F.; Zhu, H. P.; Liu, G. K.; Wu, D. Y.; Ren, B.; Tian, Z. Q. When the signal is not from the original molecule to be detected: chemical transformation of para-aminothiophenol on Ag during the SERS measurement. *J. Am. Chem. Soc.* **2010**, 132, 9244-9246.

(8) da Silva, A. G. M.; Rodrigues, T. S.; Correia, V. G.; Alves, T. V.; Alves, R. S.; Ando, R. A.; Ornellas, F. R.; Wang, J.; Andrade, L. H.; Camargo, P. H. C. Plasmonic nanorattles as next-generation catalysts for surface plasmon resonance-mediated oxidations promoted by activated oxygen. *Angew. Chem. Int. Ed.* **2016**, 55, 7111-7115.

(9) Jiang, R.; Zhang, M.; Qian, S.-L.; Yan, F.; Pei, L.-Q.; Jin, S.; Zhao, L.-B.; Wu, D.-Y.; Tian, Z.-Q. Photoinduced surface catalytic coupling reactions of aminothiophenol derivatives investigated by SERS and DFT. *J. Phys. Chem. C* **2016**, 120, 16427-16436.

(10) Devasenathipathy, R.; Wang, J.-Z.; Xiao, Y.-H.; Rani, K. K.; Lin, J.-D.; Zhang, Y.-M.; Zhan, C.; Zhou, J.-Z.; Wu, D.-Y.; Tian, Z.-Q. Plasmonic photoelectrochemical coupling reactions of para-aminobenzoic acid on nanostructured gold electrodes. *J. Am. Chem. Soc.* **2022**, 144, 3821-3832.

(11) Sun, M.; Xu, H. A novel application of plasmonics: plasmon-driven surface-catalyzed reactions. *Small* **2012**, 8, 2777-2786.

(12) Huang, Y. F.; Wu, D. Y.; Zhu, H. P.; Zhao, L. B.; Liu, G. K.; Ren, B.; Tian, Z. Q. Surface-enhanced Raman spectroscopic study of p-aminothiophenol. *Phys. Chem. Chem. Phys.* **2012**, 14, 8485-8497.

(13) Kazuma, E.; Kim, Y. Mechanistic studies of plasmon chemistry on metal catalysts. *Angew. Chem. Int. Ed.* **2019**, 58, 4800-4808.

(14) Cortés, E.; Grzeschik, R.; Maier, S. A.; Schlücker, S. Experimental characterization techniques for plasmon-assisted chemistry. *Nat. Rev. Chem.* **2022**, 6, 259-274.

(15) van Schrojenstein Lantman, E. M.; Deckert-Gaudig, T.; Mank, A. J. G.; Deckert, V.; Weckhuysen, B. M. Catalytic processes monitored at the nanoscale with tip-enhanced Raman spectroscopy. *Nat. Nano* **2012**, 7, 583-586.

(16) Sun, M.; Fang, Y.; Zhang, Z.; Xu, H. Activated vibrational modes and Fermi resonance in tip-enhanced Raman spectroscopy. *Phys. Rev. E* **2013**, 87, 020401.

(17) Zhang, Z.; Deckert-Gaudig, T.; Deckert, V. Label-free monitoring of plasmonic catalysis on the nanoscale. *Analyst* **2015**, 140, 4325-4335.

(18) Sun, J.-J.; Su, H.-S.; Yue, H.-L.; Huang, S.-C.; Huang, T.-X.; Hu, S.; Sartin, M. M.; Cheng, J.; Ren, B. Role of adsorption orientation in surface plasmon-driven coupling reactions studied by tip-enhanced raman spectroscopy. *J. Phys. Chem. Lett.* **2019**, 10, 2306-2312.

(19) Sheng, S.; Ji, Y.; Yan, X.; Wei, H.; Luo, Y.; Xu, H. Azo-dimerization mechanisms of p-aminothiophenol and p-nitrothiophenol molecules on plasmonic metal surfaces revealed by tip-/surface-enhanced raman spectroscopy. *J. Phys. Chem. C* **2020**, 124, 11586-11594.

(20) Dong, B.; Fang, Y.; Chen, X.; Xu, H.; Sun, M. Substrate-, wavelength-, and time-dependent plasmon-assisted surface catalysis reaction of 4-nitrobenzenethiol dimerizing to p,p′-dimercaptoazobenzene on Au, Ag, and Cu films. *Langmuir* **2011**, 27, 10677-10682.

(21) Xu, P.; Kang, L.; Mack, N. H.; Schanze, K. S.; Han, X.; Wang, H.-L. Mechanistic understanding of surface plasmon assisted catalysis on a single particle: cyclic redox of 4-aminothiophenol. *Sci. Rep.* **2013**, 3, 2997.

(22) Huang, Y. F.; Zhang, M.; Zhao, L. B.; Feng, J. M.; Wu, D. Y.; Ren, B.; Tian, Z. Q. Activation of oxygen on gold and silver nanoparticles assisted by surface plasmon resonances. *Angew. Chem. Int. Ed.* **2014**, 53, 2353-2357.

(23) Inagaki, T.; Kagami, K.; Arakawa, E. T. Photoacoustic observation of nonradiative decay of surface plasmons in silver. *Phys. Rev. B* **1981**, 24, 3644-3646.

(24) Baffou, G.; Quidant, R. Nanoplasmonics for chemistry. *Chem. Soc. Rev.* **2014**, 43, 3898-3907.

(25) Baffou, G.; Quidant, R.; Girard, C. Heat generation in plasmonic nanostructures: influence of morphology. *Appl. Phys. Lett.* **2009**, 94, 153109.

(26) Baffou, G.; Quidant, R. Thermo-plasmonics: using metallic nanostructures as nano-sources of heat. *Laser Photonics Rev.* **2013**, 7, 171-187.

(27) Golubev, A. A.; Khlebtsov, B. N.; Rodriguez, R. D.; Chen, Y.; Zahn, D. R. T. Plasmonic heating plays a dominant role in the plasmon-induced photocatalytic reduction of 4-nitrobenzenethiol. *J. Phys. Chem. C* **2018**, 122, 5657-5663.

(28) Sarhan, R. M.; Koopman, W.; Schuetz, R.; Schmid, T.; Liebig, F.; Koetz, J.; Bargheer, M. The importance of plasmonic heating for the plasmon-driven photodimerization of 4-nitrothiophenol. *Sci. Rep.* **2019**, 9, 3060.

(29) Zhang, Q.; Zhou, Y.; Fu, X.; Villarreal, E.; Sun, L.; Zou, S.; Wang, H. Photothermal effect, local field dependence, and charge carrier relaying species in plasmon-driven photocatalysis: a case study of aerobic nitrothiophenol coupling reaction. *J. Phys. Chem. C* **2019**, 123, 26695-26704.

(30) Lu, Y.; Wu, L.-W.; Cao, W.; Huang, Y.-F. Finding a sensitive surface-enhanced raman spectroscopic thermometer at the nanoscale by examining the functional groups. *Anal. Chem.* **2022**, 94, 6011-6016.

(31) Osawa, M.; Matsuda, N.; Yoshii, K.; Uchida, I. Charge transfer resonance Raman process in surface-enhanced Raman scattering from p-aminothiophenol adsorbed on silver: Herzberg-Teller contribution. *J. Phys. Chem.* **1994**, 98, 12702-12707.

(32) Lin, X. M.; Cui, Y.; Xu, Y. H.; Ren, B.; Tian, Z. Q. Surface-enhanced Raman spectroscopy: substrate-related issues. *Anal. Bio. Chem.* **2009**, 394, 1729-1745.

DOI: 10.14102/j.cnki.0254-5861.2022-0134

(33) Liu, G. K.; Hu, J.; Zheng, P. C.; Shen, G. L.; Jiang, J. H.; Yu, R. Q.; Cui, Y.; Ren, B. Laser-induced formation of metal-molecule-metal junctions between Au nanoparticles as probed by surface-enhanced raman spectroscopy. *J. Phys. Chem. C* **2008**, 112, 6499-6508.
(34) Kudelski, A.; Pettinger, B. SERS on carbon chain segments: monitoring locally surface chemistry. *Chem. Phys. Lett.* **2000**, 321, 356-362.
(35) Duan, S.; Ai, Y.-J.; Hu, W.; Luo, Y. Roles of plasmonic excitation and protonation on photoreactions of p-aminobenzenethiol on Ag nano-particles. *J. Phys. Chem. C* **2014**, 118, 6893-6902.
(36) Frens, G. Controlled nucleation for the regulation of the particle size in monodisperse gold suspensions. *Nature Physical Science* **1973**, 241, 20-22.
(37) Kresse, G.; Furthmüller, J. Efficient iterative schemes for *ab initio* total-energy calculations using a plane-wave basis set. *Phys. Rev. B* **1996**, 54, 11169-11186.
(38) Kresse, G.; Joubert, D. From ultrasoft pseudopotentials to the projector augmented-wave method. *Phys. Rev. B* **1999**, 59, 1758-1775.
(39) Perdew, J. P.; Burke, K.; Ernzerhof, M. Generalized gradient approximation made simple. *Phys. Rev. Lett.* **1996**, 77, 3865-3868.
(40) Methfessel, M.; Paxton, A. T. High-precision sampling for Brillouin-zone integration in metals. *Phys. Rev. B* **1989**, 40, 3616-3621.
(41) Monkhorst, H. J.; Pack, J. D. Special points for Brillouin-zone integrations. *Phys. Rev. B* **1976**, 13, 5188-5192.
(42) Duan, S.; Fang, P.-P.; Fan, F.-R.; Broadwell, I.; Yang, F.-Z.; Wu, D.-Y.; Ren, B.; Amatore, C.; Luo, Y.; Xu, X.; Tian, Z.-Q. A density functional theory approach to mushroom-like platinum clusters on palladium-shell over Au core nanoparticles for high electrocatalytic activity. *Phys. Chem. Chem. Phys.* **2011**, 13, 5441-5449.

Received: May 22, 2022
Accepted: June 11, 2022
Published online: June 20, 2022
Published: October 25, 2022

DOI: 10.14102/j.cnki.0254-5861.2022-0134